BIOCHEMISTRY
including biophysical chemistry & molecular biology
Article

Biochemistry **2009,** *48,* 12223–12232 12223
DOI: 10.1021/bi901655t

Solution Structure of a Covalently Bound Pyrrolo[2,1-*c*][1,4]benzodiazepine−Benzimidazole Hybrid to a 10mer DNA Duplex

Michael Rettig,[‡,∥] Markus Weingarth,[‡,∥] Walter Langel,[‡] Ahmed Kamal,[§] P. Praveen Kumar,[§] and Klaus Weisz*[,‡]

[‡]*Institute of Biochemistry, Ernst-Moritz-Arndt University Greifswald, Felix-Hausdorff-Strasse 4, D-17487 Greifswald, Germany, and* [§]*Chemical Biology Laboratory, Division of Organic Chemistry, Indian Institute of Chemical Technology, Hyderabad 500607, India.* [∥]*These authors contributed equally to this work.*

Received September 22, 2009; Revised Manuscript Received November 5, 2009

ABSTRACT: A pyrrolo[2,1-*c*][1,4]benzodiazepine−benzimidazole hybrid (PBD−BIMZ) derived from the tricyclic anticancer PBD antibiotics can covalently bind to a guanine base at its exocyclic 2-amino group in double-helical DNA. Through the formation of stable DNA adducts, these hybrids have previously been shown to have significant anticancer activity in a number of cell lines. Here, the three-dimensional solution structure of the complex formed between the self-complementary DNA decamer 5′-AACAATTGTT-3′ and PBD−BIMZ has been investigated by two-dimensional NMR spectroscopy and NOE distance restraint molecular dynamics simulations. Refinements using an explicit solvation model yielded a complex structure that is in good agreement with the NMR structural data. Successful convergence is indicated by an average mutual root-mean-square deviation of <1 Å for three final representative structures selected by clustering methods from the molecular dynamics trajectories at 300 K. The ligand binds in an (11*S*,11a*S*) configuration to one of the two symmetrically located guanine bases of the duplex and is oriented with its benzimidazole moiety toward the 5′-end of the modified guanine. It is accommodated within the minor groove covering the centrally located 6 bp. Conformational and helical parameters of the DNA adduct are typical of a B-like duplex, and more significant helical distortions by the covalent binding of PBD−BIMZ are mostly confined to the covalent binding site and the junction between complexed and noncomplexed DNA segments. In contrast to the overall well-determined conformation of the bound hybrid, its terminal *N*-methylpiperazine ring appears to adopt various conformations associated with increased flexibility.

Pyrrolo[2,1-*c*][1,4]benzodiazepine (PBD)[1] derivatives have been extensively studied in the past for their DNA alkylating and cytotoxic activity. Originating from various *Streptomyces* species, simple PBD drugs such as anthramycin, tomaymycin, and DC-81 belong to a family of tricyclic anticancer antibiotics that have been shown to bind to the minor groove of double-stranded DNA, forming a covalent adduct with the exocyclic amino group of a central guanine within a 3 bp recognition site (Figure 1a) (*1*−*3*). However, applications of DNA binding drugs in diagnosis, molecular biology, and medicine require small molecules with enhanced DNA binding affinity and sequence read-out, e.g., for the selective targeting of processes critical for cell proliferation. Thus, the use of pyrrolobenzodiazepine dimers with interstrand cross-linking ability (*4*, *5*) or the design of mixed PBD conjugates with a second pharmacophore linked to the PBD moiety (*6*, *7*) was driven by the need to improve the efficacy and selectivity of binding based on the expectation that the combination of two simple DNA binding agents within a single molecule would lead to an additive or synergistic activity.

Recently, a pyrrolo[2,1-*c*][1,4]benzodiazepine hybrid with a 2-phenylbenzimidazole motif tethered to the PBD moiety has been synthesized and found to be a promising inhibitor of cancer cell growth with anticancer activity in a number of cell lines (Figure 1b) (*8*). The 2-phenylbenzimidazole pharmacophore is derived from the bis-benzimidazole minor groove ligand Hoechst 33258 which has been shown to inhibit DNA topoisomerase I, binding preferentially in the DNA minor groove at stretches consisting of three or four consecutive A·T base pairs (*9*, *10*). Indeed, the PBD−benzimidazole hybrid has quite recently been shown to bind target duplexes with a preference for $(A,T)_4G$ sequences, resulting in a remarkable thermal stabilization of the double-helical oligonucleotide by up to 40 °C (*11*). However, in contrast to previous investigations of simple PBD drugs (*12*), a preference for 5′-PuGPu-3′ sequences was not apparent for the PBD hybrid in terms of binding thermodynamics as established through UV melting, fluorescence titrations, and isothermal titration calorimetry (ITC). Also, with the PBD covalently bound to a guanine base, the 2-phenylbenzimidazole moiety was found to mostly contribute to the other stabilizing noncovalent interactions between the drug and DNA. However, structural details of the formed complexes have not yet become available.

To complement the thermodynamic data on the binding of the mixed PBD conjugate to double-stranded DNA, we here present the characterization of a complex formed between a decamer

*To whom correspondence should be addressed. Telephone: +49 (0)3834 864426. Fax: +49 (0)3834 864427. E-mail: weisz@uni-greifswald.de.

[1]Abbreviations: BIMZ, 6-(4-methylpiperazin-1-yl)-2-phenyl-1*H*-benzo[*d*]imidazole; CD, circular dichroism; CPMD, Carr−Parinello molecular dynamics; DQF-COSY, double-quantum-filtered correlated spectroscopy; NOE, nuclear Overhauser enhancement; NOESY, nuclear Overhauser enhancement spectroscopy; PBD, pyrrolo[2,1-*c*][1,4]benzodiazepine; PBD−BIMZ, pyrrolo[2,1-*c*][1,4]benzodiazepine−benzimidazole hybrid; RESP, restrained electrostatic potential; rMD, restrained molecular dynamics; rmsd, root-mean-square deviation; TOCSY, total correlation spectroscopy.

Published on Web 11/13/2009

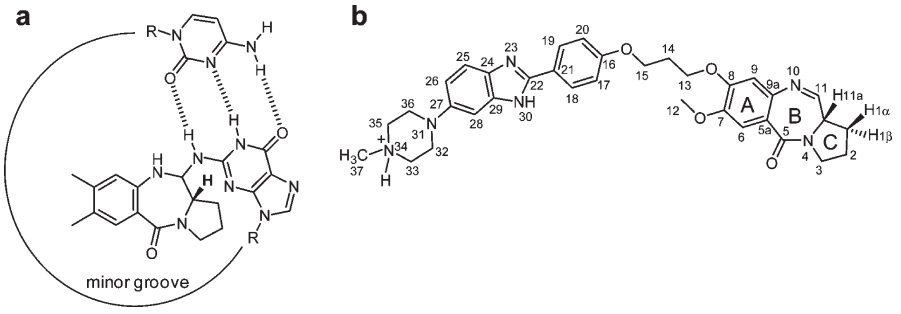

FIGURE 1: Structure of a pyrrolobenzodiazepine−dG·dC adduct (a) and of the pyrrolo[2,1-*c*][1,4]benzodiazepine−benzimidazole hybrid with atom numbering (b).

duplex and the hybrid drug using NMR spectroscopy and restrained molecular dynamics calculations. There have been several structural studies on DNA adducts with monomeric or dimeric PBD ligands in the past (*13*−*15*). These studies have established formation of a covalent bond between the PBD and the exocyclic 2-amino group of guanine bases with the PBD A-ring oriented toward the 3′-terminus of the alkylated strand. This work provides for the first time a three-dimensional structure of a DNA adduct with a chimeric PBD ligand revealing distinct differences in the adduct geometry when compared to the duplex binding of simpler PBD drugs. It thus gives important insight into drug−DNA interactions within such complexes, a prerequisite for the future rational design of PBD conjugates with improved binding characteristics.

MATERIALS AND METHODS

Sample Preparation. The self-complementary 10mer deoxyribonucleotide 5′-AACAATTGTT-3′ purchased from *TIB MOLBIOL* (Berlin, Germany) was dissolved in BPS buffer [100 mM NaCl and 20 mM phosphate (pH 7.0)]. The drug−DNA complex was prepared by titrating the DNA duplex in 0.5 mL of buffer with a total of 20 μL of a concentrated drug solution in DMSO-d_6 until saturation. For NMR experiments with exchangeable protons, samples in a 90% H_2O/10% ^2H_2O mixture were used. For experiments with nonexchangeable protons, the NMR sample was lyophilized twice and redissolved in 99.98% D_2O. The final buffer solution for the NMR studies was ~0.7 mM in duplex.

NMR Experiments. ^{1}H NMR experiments were performed on a Bruker Avance 600 MHz spectrometer. A combination of phase-sensitive nuclear Overhauser effect spectroscopy (80, 140, and 200 ms mixing time NOESY) as well as through-bond-correlated (COSY, phase-sensitive DQF-COSY) and total correlated spectroscopy (50, 80, and 120 ms spin lock time TOCSY with DIPSI2 or MLEV17 and a field strength of 4.9 kHz) was applied for the samples in the States−TPPI mode except for magnitude mode COSY experiments. Typically, for assignments of nonexchangeable protons, two-dimensional (2D) spectra in D_2O were recorded at 295 K with a sweep width of 6600 Hz and the carrier frequency was set to the HDO resonance frequency. Residual HDO was suppressed with a 3-9-19 WATERGATE sequence or by presaturation during the relaxation delay as required. A total of 512 FIDs of 2048 complex data points were collected in t_1 with 64 transients at each t_1 value and a recycle delay of 2 s. Prior to Fourier transformation, the FIDs were zero-filled to give a 2K × 2K or 2K × 1K data set. Both dimensions were apodized with phase-shifted sine or squared sine-bell functions. Proton chemical shifts were referenced to the HDO peak taking into account the temperature dependence of its chemical shift (*16*).

For the assignments of exchangeable protons, 2D NOE experiments in a 90% H_2O/10% ^2H_2O mixture were conducted at 283 K with a 200 ms mixing time and a spectral width of 14300 Hz using either the DPFGSE or the 3-9-19 WATERGATE pulse sequence for solvent suppression. Corresponding suppression schemes were also used for one-dimensional (1D) experiments in H_2O buffer.

Distance Restraints. For an evaluation of cross-peak intensities, NOE spectra in D_2O with and without presaturation during the relaxation delay and acquired with a short 80 ms mixing time to avoid significant spin diffusion effects were employed. Also, the relaxation delay was increased to 5 s to allow for a better spin equilibrium. For obtaining distance restraints within the two-spin approximation, SPARKY (*17*) was used to directly calibrate cross-peak intensities against an average intensity of the cytosine H5−H6 (2.45 Å) cross-peak. All cross-peaks were subsequently assigned to one of six categories. Five categories are based on peak intensities, and one category was set up to include both overlapping resonances and resonances of exchangeable protons. The restraints for the exchangeable protons were directly derived from the spectra used for the proton assignments. A flat-well potential was imposed for the experimental restraints; i.e., no penalty is imposed on the system between lower and upper bounds (r_2 and r_3, respectively). Beyond this target range, the potential function rises parabolically, until for even wider lower and upper margins ($r_1 = r_2 - 0.5$ Å and $r_4 = r_3 + 0.5$ Å, respectively) the penalty function continues linearly to avoid exceedingly high energies for larger violations. For the lower bound, the van der Waals radii of 1.8 Å were used. The upper bounds were set to 3.0, 4.0, 4.5, 5.0, and 5.5 Å depending on the cross-peak intensities and 5.0 Å for overlapping resonances and all exchangeable protons. These conservative distance estimates avoid overinterpretation of the data and reduce the potential for inconsistencies among restraints. For the Watson−Crick (WC) hydrogen bond restraints, r_2 and r_3 values were obtained from ref *18*, allowing 0.2 Å fluctuations from the equilibrium bond distance. In addition, flat angle restraints with angles between the three atoms forming a Watson−Crick hydrogen bond were set to 170−190° with parabolic regions extending on either side for 20°.

Model Building and Parametrization. The self-complementary 10mer d(AACAATTGTT)$_2$ was built in its canonical B-form using the NUCGEN application of the modeling program package AMBER version 9 (*19*). Initial coordinates of the PBD−benzimidazole hybrid were taken from the B3LYP/6-31G* optimized geometry calculated in vacuum with GAUSSIAN 03

(Gaussian, Inc., Wallingford, CT). On the basis of the NMR data (vide infra), the hybrid was hand-docked into the minor groove of the DNA with the PBD moiety of the drug covalently linked to the single guanine base on one of the two strands using AMBER's XLeap module. This procedure was repeated starting with a canonical A-DNA to yield two independent starting geometries. The refined PARMBSC0 force field of AMBER was used to simulate the DNA as well as solvent and sodium ions (*20*). For the drug, general AMBER force field GAFF (*21*) was employed using RESP charges (*22*, *23*) computed at the HF/6-31G* level on the B3LYP/6-31G*-optimized geometry.

Simulated Annealing. The system was initially minimized using the conjugate gradient algorithm to eliminate strong restraint violations. The simulated annealing was conducted in water using a generalized Born implicit solvent model with implicit counterions (*24*, *25*). The minimized starting complexes were initially heated to 900 K and kept at this temperature for 26 ps. During the next 50 ps, the system was gradually cooled to 100 K and the temperature set to 0 K for the last 2 ps. The force constants were initially 1.5 kcal mol^{-1} Å^{-2} for NMR restraints as well as 2.5 kcal mol^{-1} Å^{-2} and 2.5 kcal mol^{-1} rad^{-2} for Watson−Crick distance and flat angle restraints, respectively. They were linearly increased during the first 22 ps to their final values of 30 and 50 kcal mol^{-1} Å^{-2} and 50 kcal mol^{-1} rad^{-2}, respectively. A minimization completed the simulated annealing run. All Watson−Crick restraints were removed before subsequent simulations in explicit solvent.

After charge neutralization by the addition of 17 Na^+ ions, the complexes were solvated with 4000 pre-equilibrated TIP3P water molecules in a truncated octahedral box (*26*). Several equilibration steps were performed comprising minimization of the solvent molecules with the DNA and ligand fixed, minimization of the whole system, and slow heating to 300 K with weak positional restraints on DNA and drug atoms under constant-volume conditions. The following 15 ns production runs were applied in the NPT ensemble. The particle mesh Ewald method (*27*, *28*) was used to evaluate the electrostatic interactions with a direct space sum cutoff of 10 Å. With the bond lengths involving hydrogen atoms kept fixed with the SHAKE algorithm, a time step of 2 fs was employed (*29*).

Structural Analysis and Display. Related conformational substates populated during the molecular dynamics simulation were grouped by clustering using the SOM algorithm implemented in AMBERS's PTRAJ module (*30*). For the clustering, only the piperazine and benzimidazole ring atoms were chosen for a pairwise comparison (vide infra). All structures within a cluster were averaged, and the average configuration was taken as a reference for subsequent mass-weighted rmsd calculations with terminal base pairs omitted. The single snapshot of the given cluster with the lowest rmsd was taken as the representative dynamic structure of that cluster. All structures were displayed with VMD version 1.8.6 (*31*). Analysis of the conformational and helical parameters was conducted with Curves version 5.3 (*32*, *33*).

Carr−Parinello Molecular Dynamics (*CPMD*). CPMD version 3.9.1 (IBM Corp. and MPI, Stuttgart, Germany) was used to test the time-dependent behavior of the BIMZ fragment. The fragment was placed in a periodic vacuum box (x,y,z) = (41.572 Å, 24.527 Å, 24.527 Å), heated in six discrete steps from 0 to 300 K over 510 fs, and simulated over 3.4 ps at this temperature. The pseudopotentials of Troullier-Martins (*34*) and a cutoff of 25 Ry were employed. For the local density approximation (LDA) and the generalized gradient approximation (GGA), the methods of Cerperley-Alder and Becke88 were used (*35*).

RESULTS AND DISCUSSION

^{1}H NMR Resonance Assignments of Free DNA. On the basis of the significant duplex thermal stabilization on drug binding (*11*) and a favorable NMR signal dispersion, the self-complementary DNA duplex d(AACAATTGTT)$_2$ carrying two symmetry-related guanine bases was selected as a target for the drug hybrid. In the following, residues of the decamer duplex are numbered according to

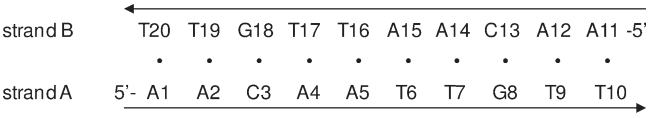

Note that due to the 2-fold symmetry of the free duplex, strands A and B are equivalent without bound drug. Nonexchangeable protons were assigned by analyzing 2D NOE (200 ms mixing time) and TOCSY (80 ms spin lock time) spectra following established strategies (*36*, *37*). The sequential assignment of most base and sugar protons was mainly based on continuous base-to-sugar proton dipolar coupling networks, and protons of the deoxyribose sugar were additionally identified by their mutual scalar couplings. Likewise, assignment schemes for labile protons are based on their connectivities to other exchangeable and nonexchangeable protons in H_2O solution (*38*). Because of enhanced proton exchange with water toward the fraying end of the DNA duplex, imino proton resonances of the terminal base pairs were broadened beyond detection. The overall pattern of NOE cross-peaks and their relative intensities are consistent with a right-handed double helix, a glycosidic torsion angle in the anti range, and an S-type sugar pucker characteristic of B-DNA (*39*). A compilation of all proton chemical shifts for the free duplex is given as Supporting Information.

^{1}H NMR Resonance Assignments of the Drug−DNA Complex. Upon binding as a monomer to the DNA, the asymmetric PBD hybrid is expected to break the symmetry of the free duplex. Correspondingly, titration of the duplex with drug is associated with a doubling of the oligonucleotide proton resonances (Figure 2). As mentioned above, only four imino protons are observed for the free duplex due to the terminal imino signal being broadened beyond detection.

After the addition of 1 equiv of hybrid associated with the appearance of seven sharp as well as two rather broad imino signals, no further spectral changes are observed in line with the saturation of DNA with drug. With the addition of less than saturating amounts of PBD−BIMZ, two sets of resonances appear, one of which corresponds to that of the free DNA and the other to the 1:1 drug−DNA complex. This observation indicates that the complex is in slow exchange with the decamer duplex on the NMR time scale.

For the assignment of the DNA resonances in the complex, the same established strategies as for the free duplex were employed, allowing an assignment for most of the nonexchangeable and exchangeable protons except for the H5′/H5″ protons that were mostly left unassigned due to severe spectral overlap. The single guanine N2H proton at the covalent attachment site resonating at 8.09 ppm was easily observable in H_2O and could be identified through its strong NOE cross-peak to the guanine imino proton.

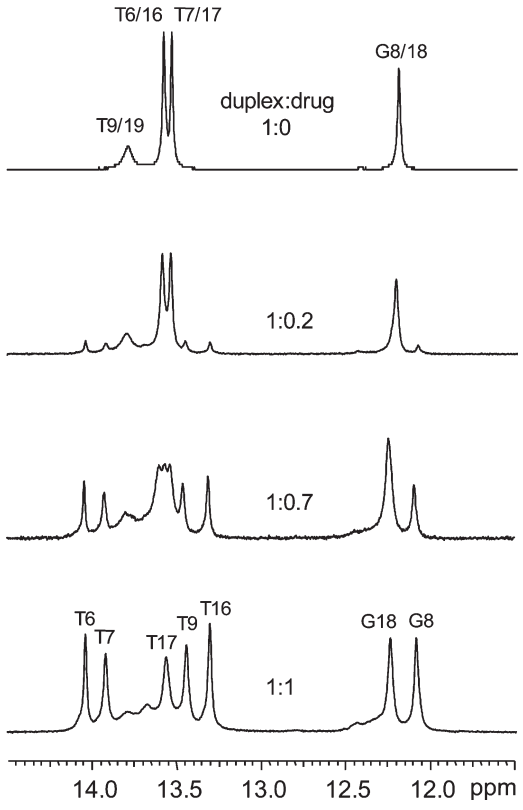

FIGURE 2: Imino proton spectral region during titration with the drug at 283 K.

Again, the general pattern of NOE intensities suggests a B-type DNA for the complex, and only some sequential and intranucleotide NOE contacts of very low intensity at nucleotides G18 and T6 in the base−H1′ cross-peak spectral region point to some perturbations of the typical B-like helical structure. Rather low intensities of additional sequential and intraresidual cross-peaks involving the latter two residues suggest enhanced flexibility at these positions rather than defined structural aberrations. The assignment of the adenine H2 protons that are exposed to the minor groove and thus particularly important in defining the location of minor groove binding drugs was additionally confirmed by their comparatively long spin−lattice relaxation time as measured in 1D inversion recovery experiments.

Drug resonances were mostly identified through their scalar connectivities within the corresponding spin system. Thus, the aromatic protons of the benzene moiety in the BIMZ fragment were easily assigned through COSY and in particular TOCSY spectra. Likewise, proton resonances of the linker region, of the pyrrolidine, and of the *N*-methylpiperazine ring were identified via their correlations in TOCSY spectra. Remaining resonances of the PBD fragment were assigned via NOESY spectra. Unfortunately, except for H28, it was not possible to unambiguously assign the benzimidazole resonances mainly due to spectral overlap. To avoid any misinterpretation of the final data, these questionable NOE contacts were excluded for the final extraction of NMR restraints. All proton chemical shifts for the drug−DNA adduct are given as Supporting Information.

NMR Spectral Analysis. The ^3J scalar coupling between H11 and H11a of the pyrrolobenzodiazepine moiety bears particular importance when the stereochemistry of drug binding is being assessed (vide infra). Only one scalar coupling associated with a single COSY cross-peak is observed in a D_2O solution for the H11 proton resonating at 4.61 ppm. In contrast, the H11a resonance at 5.02 ppm exhibits an additional coupling to a vicinal H1 proton of the pyrrolo ring at 2.22 ppm. A closer look at the DQF-COSY cross-peaks along the well-resolved ω_2 dimension reveals a characteristic fine structure amenable to a quantitative extraction of scalar coupling constants. A ^3J(H11,H11a) of $\sim 10 \pm 0.5$ Hz is extracted from the two well-separated antiphase components along ω_2 of the H11a(ω_1)−H11(ω_2) cross-peak. An additional smaller in-phase splitting for the H11(ω_1)−H11a(ω_2) cross-peak yields a ^3J(H11a,H1) of $\sim 6 \pm 1$ Hz (see the Supporting Information). Without resorting to quantitative simulations, cancellation and amalgamation effects for antiphase and in-phase splittings in the latter case hamper a more precise coupling constant determination. Note also that the absence of any additional coupling between H11a and the other geminal H1 pyrrolo proton must result from a rather small nonresolved coupling only contributing to the signal line width.

Several intermolecular NOE contacts clearly establish drug binding in the duplex minor groove. Thus, a large portion of observable drug−DNA connectivities involve adenine H2 and H1′/H4′ sugar protons situated at the floor and the walls of the minor groove, respectively (see Figure 3). A comparison of chemical shifts for protons in the free PBD hybrid with those in the complex also reveals some significant differences. Thus, the largest upfield shift with a $\Delta\delta$ of 3 ppm was observed for the H11 resonance of the PBD moiety, and this was followed by a downfield shift of 1.3 ppm for the adjacent H11a signal upon DNA binding. Although reference spectra of the free drug were recorded in DMSO-d_6 because of its poor solubility in aqueous buffer, effects of solvent on chemical shifts as indicated by changes in the other drug protons do not account for such considerable differences. Rather, the observed significant upfield shift for the H11 signal must be attributed to covalent binding of the drug with addition of a guanine amino group to the PBD imine functionality accompanied by a change in C11 hybridization from sp^2 to sp^3.

Significant shifts were also observed for some of the DNA resonances upon drug binding (Figure 4). Among the anomeric H1′ protons of the DNA duplex, the largest drug-induced upfield shift with a $\Delta\delta$ of 1.03 ppm was observed for H1′ of G8, resonating at an unusually high field in the complex with a δ of 4.93 ppm and already pointing to this guanine as a site of covalent adduct formation. Also, H4′ of T6 and H4′ of T17 facing the minor groove exhibit considerable upfield shifts of >1 ppm. Conspicuously, deoxyribose protons of residue T17 are found to be mostly affected by shielding effects of the bound drug. Thus, other major upfield shifts of >0.6 ppm involve H1′ and H2″ sugar protons of T17. This is readily apparent from Figure 4a, which shows a footprint of the bound drug constructed by the sum of chemical shift changes for sugar protons within the residues regardless of sign. In general, excluding largely non-assigned H5′/H5″ protons, H3′ protons oriented toward the major groove of the duplex are found to be the least affected of the sugar protons. Note that although heavily affected in some residues, H4′ protons have been excluded for the footprint mapping because their unambiguous assignment is lacking for three nucleotides in the complex.

In contrast to the most affected sugar resonances, adenine H2 protons from inner residues A4, A5, A14, and A15 positioned at the floor of the minor groove experience a considerable drug-induced deshielding with a downfield shift of up to 0.65 ppm for H2 of A5 (Figure 4b). Overall, noticeable shifts indicative of

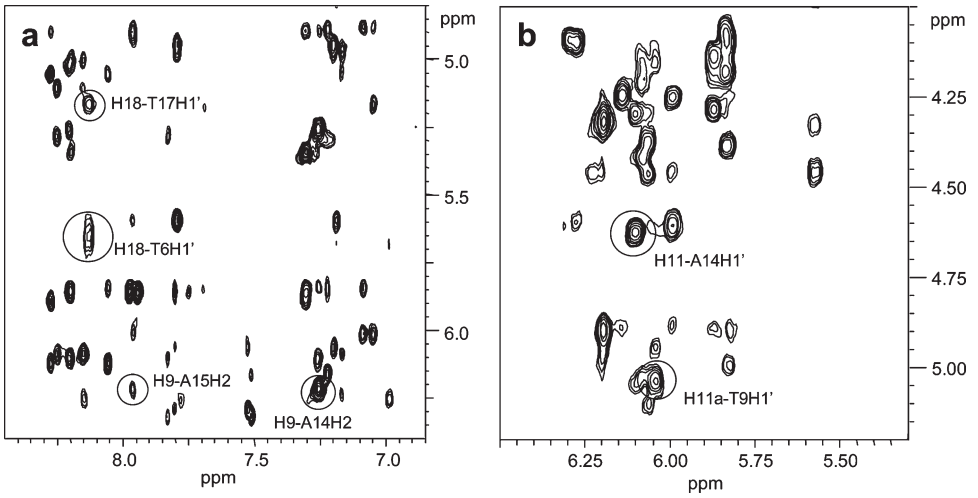

FIGURE 3: (a) Aromatic−H1′ and (b) H1′−H3′, −H4′, −H5′, and −H5″ 2D NOE spectral region of the complex (80 ms mixing time, 295 K) with contacts between drug and H1′ protons indicated.

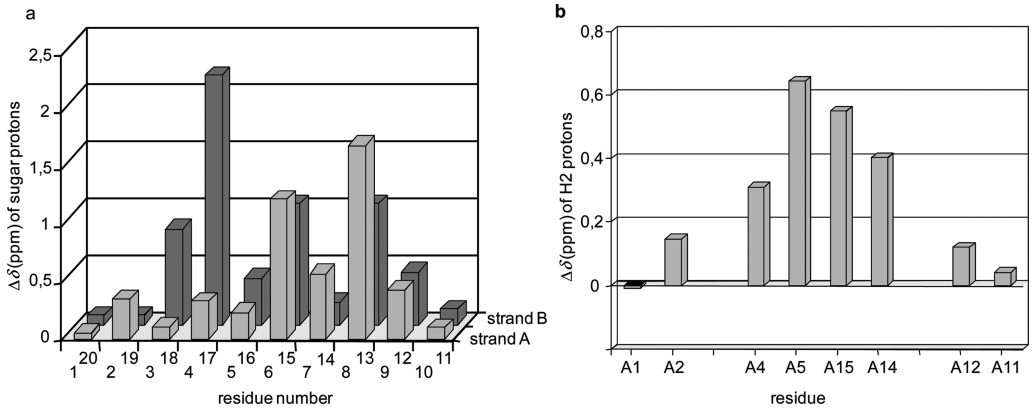

FIGURE 4: ^{1}H chemical shift changes ($\Delta\delta = \delta_{complex} - \delta_{duplex}$) for DNA protons. (a) Sum of $\Delta\delta$ values for H1′, H2′, H2″, and H3′ deoxyribose protons irrespective of upfield or downfield shift. (b) Adenine H2 base protons.

direct drug−DNA interactions are restricted to resonances within the inner 6 bp of the complex.

2D NOE Restraints. A total of 237 distance restraints, including 206 NOE contacts between nonexchangeable and exchangeable protons within the DNA duplex and 28 drug−DNA contacts, were extracted. NOE restraints with fixed distances were not included. The 44 Watson−Crick restraints are based on the slowly exchanging guanosine and thymidine imino protons showing NOE connectivities to cytidine amino and adenosine H2 protons consistent with a nondisrupted Watson−Crick base pair. Although no such contacts could be detected for the terminal imino signals because of their fast exchange with the solvent (vide supra), corresponding restraints were also imposed for the termini to avoid base pair opening during the simulated annealing protocol. However, all Watson−Crick restraints were removed for the final refinement in explicit water.

The intraduplex restraints are uniformly distributed along the two strands except for the less well-defined flexible termini. Each residue except for the terminal base pairs was restricted by ≥17 intra- and internucleotide restraints. A total of 28 drug−DNA restraints and 3 intradrug restraints, which also help to define the position of the trimethylene linker within the hybrid, could be obtained. Whereas the orientation of the PBD moiety was well-defined by proton−proton contacts with the duplex, no additional drug−DNA restraints were used in the rMD simulations for the benzimidazole and the *N*-methylpiperazine moiety. As described above, resonances could not be unambiguously assigned for the benzimidazole due to spectral overlap. On the other hand, rather broad proton resonances of the *N*-methylpiperazine indicated a significant intrinsic flexibility of this ring system preventing the detection of any intermolecular cross-peaks to the DNA even at a lower temperature of 283 K.

Starting Structures and Stereochemistry. To sample more conformational space, two independent rMD simulations for either a B- or A-DNA starting geometry were performed. Note, however, that for both starting structures the drug was already partly fixed due to the covalent bonding of the PBD fragment to the exocyclic amino group of G8. This covalent bond of the pyrrolobenzodiazepine to the guanine base generates another stereogenic center at C11 of the drug. With an *S*-configuration at C11a, known to be prerequisite for the accommodation of PBD drugs within the DNA minor groove, two potential diastereoisomers, (11*S*,11a*S*) and (11*R*,11a*S*), may be formed during formation of the complex. In geometry-optimized structures of PBD−9-methylguanine adducts at the B3LYP/6-31+G** level, dihedral angles between H11 and H11a protons in the two different configurations show significant differences with angles of ∼165° and ∼75° for the (11*S*,11a*S*) and the (11*R*,11a*S*) diastereoisomers, respectively. On the basis of the general Karplus relationship, a corresponding vicinal ^{1}H−^{1}H ^{3}J coupling

constant of ~10 Hz determined from DQF-COSY experiments essentially excludes torsion angles in the range of 20−140°, thus being only compatible with an (11*S*,11a*S*) isomer even considering some uncertainties associated with the lack of a PBD-optimized Karplus equation and some conformational flexibility of the seven-membered ring. This stereochemical assignment is further confirmed by interatomic distances between H11a and H11 drug protons and anomeric H1′ protons of the duplex A- and B-strand, serving as additional diagnostic markers for the C11 configuration of the bound drug (*40*, *41*). As shown in Figure 3, NOESY spectra clearly establish strong cross-peaks between H11a and H1′ of residue T9 3′-linked to the alkylated guanosine as well as between H11 and A14 H1′ on the complementary strand. These experimental observations provide evidence of corresponding interproton distances of <5 Å in the DNA−drug adduct and are again only compatible with an (11*S*,11a*S*) configuration (vide infra). Indeed, when starting with an (11*R*,11a*S*) isomeric drug, which has been independently parametrized before, considerable violations of these NOE distances associated with unreasonable conformations were generated in additional rMD test simulations.

General Characterization of the rMD-Refined Structures. An rmsd plot over the two trajectories of the final refinements in explicit water indicates full equilibration of the system after approximately 1.5 ns. However, visual inspection of the molecular configurations from the rMD simulations revealed conspicuously different orientations of the drug−piperazine ring. To further explore the sampled conformations, the two trajectories obtained after the initial equilibration period were merged and subjected to a cluster analysis using the rmsd values of the piperazine and benzimidazole atoms as clustering criteria. As indicated by the quality metrics for the SOM clustering algorithm and supported by a visualized 2D rmsd plot (see the Supporting Information), partitioning of the data into three distinct clusters best reproduces the various populated configurations.

A best fit superposition of the representative configurations for each of the three clusters (see Materials and Methods) is shown in Figure 5. Except for the duplex termini and a less well-defined *N*-methylpiperazine orientation of the bound drug due to its conformational variability, the complexes have converged essentially to the same geometry even with the rather conservative bounds employed for the NMR restraints. When the piperazine ring and the more flexible ultimate base pairs are excluded, mutual rmsds among the three dynamic complexes are below 1 Å (see Table 1). Such deviations involving independent refinements are comparable to the magnitude of atomic rms fluctuations during a single converged rMD run in the present force field and thus imply structural convergence. In addition to the rather small rmsds, the restraint violations indicate a good agreement of the generated structures with the experimental NMR data. Thus, the average restraint violation energy calculated for the three representative structures amounts to only 1.3 kcal/mol with only one violation >0.1 Å. It should be noted that upon an additional restrained energy minimization, violation energies essentially vanish.

Structural Analysis. With all three representative structures having essentially the same conformation, only the structure of the most populated cluster was used for a more detailed structural analysis. To eliminate random thermal fluctuations within the complex, the dynamic structure was relaxed through a final restrained energy minimization. As shown by the energy-minimized representative structure of the DNA−drug adduct in Figure 6, the PBD−benzimidazole hybrid is tightly accommodated within the minor groove of the duplex and spans the centrally located 6 bp.

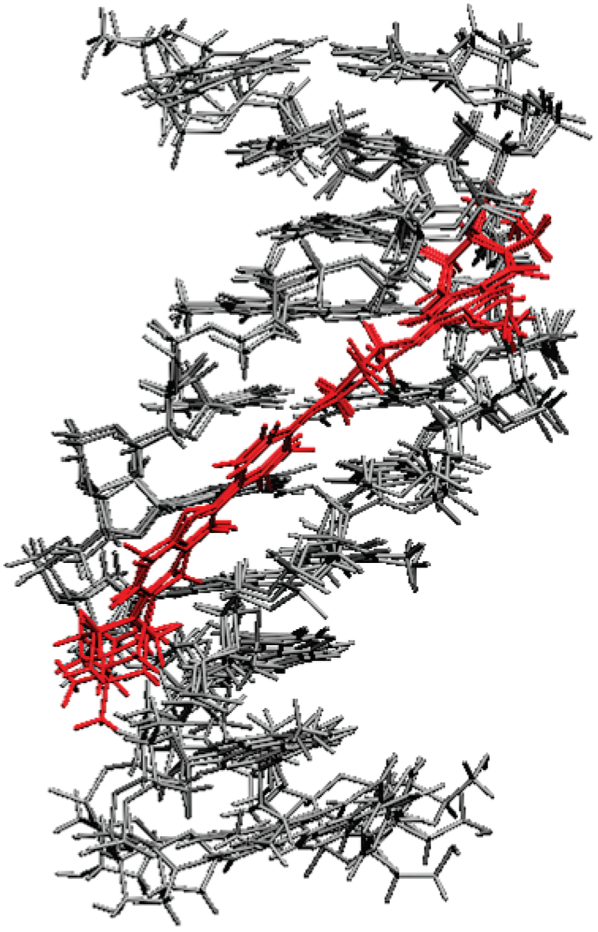

FIGURE 5: Best fit superposition of the three representative complex structures after rMD refinement at 300 K. The PBD hybrid located in the duplex minor groove is colored red.

Table 1: Statistical Data for the NMR Restraints and for the Three Representative Structures Selected by Clustering Methods after Refinement in Explicit Water at 300 K

total no. of experimental NOE restraints	237
duplex intraresidual restraints	87
duplex interresidual restraints	102
duplex interstrand restraints	17
duplex Watson−Crick H bond restraints	44
intermolecular drug−duplex restraints	28
intramolecular drug restraints	3
average rmsd (all atoms excluding ultimate base pairs)	0.93 Å
average rmsd (all atoms excluding ultimate base pairs and *N*-methylpiperazine)	0.84 Å
average restraint violation energy	1.3 kcal/mol
average no. of distance violations of <0.1 Å	2
average no. of distance violations of >0.1 and <0.2 Å	1

When the bound drug and the ultimate base pairs are excluded, the mutual rmsds between the energy-minimized duplex and A- and B-DNA starting models amount to 4.4 and 1.7 Å, respectively. Clearly, the duplex in the presence of bound drug remains in a conformation more reminiscent of B-DNA, and the A-DNA starting structure easily converged during the production run following the simulated annealing protocol to the final B-type

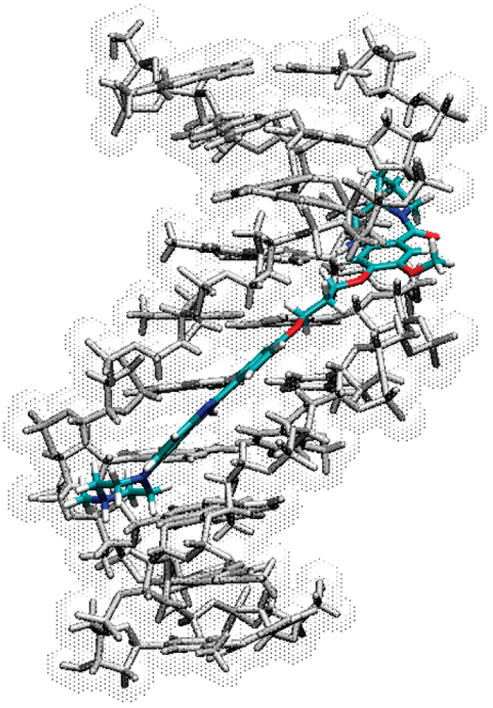

FIGURE 6: Representative energy-minimized structure of the complex showing the drug bound within the DNA minor groove.

complex even in the absence of additional torsion angle restraints for the deoxyribose. This is also manifested in the conformational and helicoidal parameters of the duplex being mostly within the broader range observed for B-DNA structural variants. Glycosidic torsion angles κ for nonterminal nucleotides adopt typical values in the anti domain varying from $-101°$ to $-145°$, and the deoxyribose sugars exhibit a largely S-type conformation.

Conspicuous structural distortions due to drug binding, as also indicated by CD spectral data (*11*), are largely confined to some helicoidal parameters around the covalent binding site (see Table 2). Thus, with a stagger of -0.6 Å, the modified guanine is noticeably displaced along the helix axis within the base pair. This is accompanied by a significant propeller twist of $-22°$ for the G8·C13 base pair. The maximum propeller twist of $-28°$ found for the neighboring T9·A12 base pair helps to maximize stacking interactions with the alkylated G·C base pair. In contrast, stacking interactions of the G8·C13 base pair with the next base pair located toward the center of the helix is considerably compromised by a linear *x*-displacement between the two base pairs with a shift of the T7·A14 base pair toward the major groove by -1.2 Å. Other structural perturbations are noticeable at the transition from free to complexed segments of the duplex. Thus, a significant positive buckle at the C3·G18 base pair bends the center of this base pair away from the center of the double helix, and a positive roll of 12° between the A4·T17 and C3·G18 base pairs results in an opening toward the major groove and a concomitant local expansion of the minor groove at the *N*-methylpiperazine location. Overall, with an average twist angle of 34°, the duplex is slightly underwound in the presence of the drug when compared to canonical B-DNA. Also, a narrowing of the minor groove is observed along the ligand binding site. A narrow minor groove is generally associated with AT tracts but is also promoted among others by the positive base pair opening values throughout the duplex with opening toward the major groove.

Table 2: Helical Parameters[a] for the Representative Energy-Minimized Complex Structure[b]

base pair	shear (Å)	stretch (Å)	stagger (Å)	buckle (deg)	propeller twist (deg)	opening (deg)
A2·T19	0.2	0.2	0.0	6	−14	0
C3·G18	−0.3	0.2	0.2	14	−14	3
A4·T17	0.1	0.1	−0.5	4	−25	2
A5·T16	0.1	0.3	0.2	−6	−11	10
T6·A15	0.0	0.1	0.5	0	−12	5
T7·A14	0.1	0.1	0.0	9	−1	3
G8·C13	−0.1	0.1	−0.6	−5	−22	2
T9·A12	−0.5	0.2	−0.3	−9	−28	8
average	0.0	0.2	−0.1	1	−16	4
B-DNA[c]	0.0	0.0	0.1	0	4	−4

base pair step	shift (Å)	slide (Å)	rise (Å)	tilt (deg)	roll (deg)	twist (deg)
A2C3·G18T19	0.8	−0.2	3.2	−4	−2	27
C3A4·T17G18	−0.5	0.1	3.5	1	12	37
A4A5·T16T17	0.7	−0.7	3.6	−3	3	29
A5T6·A15T16	0.0	−0.1	3.4	1	−3	36
T6T7·A14A15	0.3	0.0	3.2	6	−9	32
T7G8·C13A14	−1.2	0.2	3.6	0	5	36
G8T9·A12C13	0.6	−0.7	3.1	−2	2	31
average	0.1	−0.1	3.3	0	0	34
B-DNA[c]	0.0	0.0	3.4	0	0	36

[a]Individual parameters are defined with respect to a unique global helix axis. [b]Terminal base pairs were omitted. [c]Canonical B-DNA (*42*).

Stereochemistry and Drug−DNA Interactions. As a result of the newly created stereogenic center at C11 with its *S*-configuration, the H11a and H11 protons are situated above and below the PBD ring system in the proximity of T9 and A14 H1′ sugar protons, respectively (Figure 7a). Corresponding distances of only 2.4 and 2.7 Å are in line with the strong NOE contacts observed experimentally. Also, torsion angles of 175° between H11 and H11a and 32° and 90° between H11a and the two geminal H1α and H1β pyrrolo protons, respectively, are in excellent agreement with measured ^{1}H−^{1}H coupling constants (vide supra).

In previous studies on the DNA binding of the PBD drug tomaymycin, two conformational forms were found and assigned to the (11*S*,11a*S*) and (11*R*,11a*S*) diastereomeric adducts binding in opposite orientations within the minor groove (*43*). In general, however, an 11*S* stereochemistry has mostly been found to be favored for covalent attachment of simple PBD monomers or interstrand cross-linking dimers in the minor groove of duplex DNA and the C11(*S*) linkage seemed to be associated with an orientation of the aromatic A ring of the PBD drug toward the 3′-side of the covalently modified guanine (*40*, *41*, *44*). Because of its size, the PBD hybrid in this adduct can only orient in an opposite direction with the A ring toward the 5′-end of the modified guanine strand for effective minor groove binding of the BIMZ moiety and thus contrasts with the previously found dependence of drug orientation on stereochemistry.

Major shielding and deshielding effects experienced by DNA protons upon drug binding (vide supra) can be rationalized by the three-dimensional complex structure and must be attributed to strong ring current effects exerted by the hybrid ligand. With the aromatic rings of the hybrid inserted edge-on into the minor groove, upfield ring current effects are expected in particular for the deoxyribose protons that form the walls of the minor groove and that are positioned above or below the π-plane of the

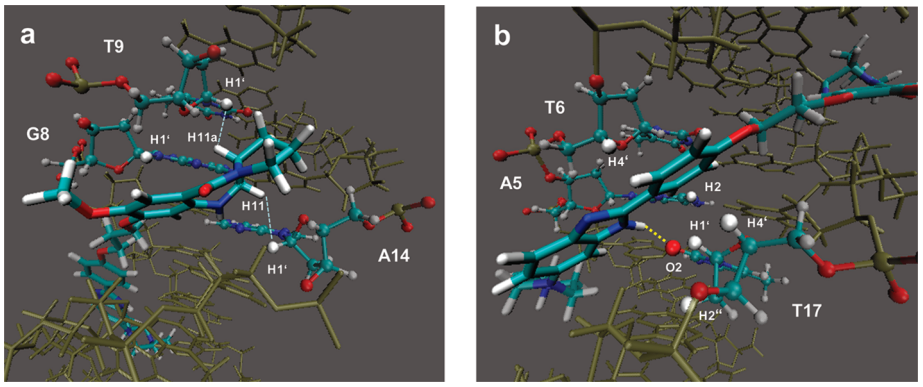

FIGURE 7: Close-up views into the minor groove of the drug−DNA complex. (a) PBD moiety with H1′ protons in spatial proximity. (b) Phenylbenzimidazole fragment with highlighted DNA protons experiencing strong (de)shielding effects. The hydrogen bond between the benzimidazole NH proton and the 2-carbonyl oxygen of T7 is indicated by the dotted line.

aromatic rings. As shown in Figure 7b, shielding of the T6 H4′ sugar proton located directly above the benzene moiety of the phenylbenzimidazole fragment is expected and observed. Likewise, T17 H4′, T17 H1′, and T17 H2″ protons are strongly shielded by their location below the benzene and benzimidazole plane, respectively. Another strong ring current effect is experienced by the anomeric H1′ proton of the alkylated G8 situated above the annellated benzene of the PBD tricyclic system (see Figure 7a). In contrast to these strongly shielded resonances, the adenine H2 protons are positioned on the floor of the minor groove and experience noticeable downfield perturbations to their chemical shifts when located close to the deshielding region of the hybrid aromatic ring systems. This is apparent for A5 H2 exhibiting a downfield shift by 0.65 ppm through its location within the benzene plane of the drug (Figure 7b).

A hydrogen bond between the PBD NH10 group and N3 of A14 is indicated by a distance of 2.0 Å in the final energy-minimized structure, and this interaction persists through most of the rMD simulations based on a critical hydrogen bond distance of <3.5 Å. Hydrogen bond analysis of the complex reveals another strong hydrogen bond with a distance of 1.9 Å between the benzimidazole NH proton of the hybrid as a donor and the 2-carbonyl oxygen of T17 as a hydrogen bond acceptor (Figure 7b). This hydrogen bond interaction is also maintained in the trajectories at 300 K. The noticeably reduced binding affinity and duplex thermal stabilization as recently observed for the drug when bound to double-helical targets with only three contiguous A·T base pairs upstream the GC site (*11*) may be partially attributed to the loss of this hydrogen bond contact. Although the two hydrogen bonds are expected to confer sequence selectivity to binding due to their directionality, they will hardly constitute the major factor in the overall binding energy of the enthalpy-driven (*11*) association. Rather, the tight structural fit of the drug within the duplex minor groove points to significant van der Waals interactions as a major enthalpic contribution to the hybrid binding. These observations corroborate the finding that in many cases minor groove recognition is not predominantly controlled by the formation of specific hydrogen bonds and salt bridges but is rather accompanied by significant hydrophobic forces (*11*, *45*, *46*). Thus, the endothermic binding of the bis-benzimidazole Hoechst 33258 to oligonucleotide duplexes was found to be exclusively driven by hydrophobic effects (*47*).

Conformation of the N-Methylpiperazine Ring. The *N*-methylpiperazine ring is located close to the second G·C base pair within the wider minor groove. As already indicated, conformational transitions associated with a less well-defined orientation are observed for the *N*-methylpiperazine moiety of the drug (see Figure 5). Whether these different conformations are due to its intrinsic flexibility or rather due to the lack of additional inter- or intramolecular NOE restraints for the piperazine ring cannot be answered with certainty. However, its inherent flexibility and dynamics are corroborated by corresponding proton resonances experiencing some noticeable line broadening.

To gain additional information about the orientation and the inherent flexibility of the benzimidazole−*N*-methylpiperazine subunit in the absence of more NMR structural data, a first principles molecular dynamics treatment with CPMD was applied to the BIMZ fragment. In contrast to that of the benzimidazole, the orientation of the directly bonded benzene moiety with respect to the DNA minor groove is well-defined by the available NOE data. Due to π-conjugation between the benzimidazole and the benzene ring of the BIMZ fragment, both rings are expected to share a common molecular plane. Indeed, CPMD simulations conducted at 300 K over 3.4 ps clearly indicate coplanarity with no ring flipping occurring during the trajectory. Similarly, high-resolution structures of DNA-bound Hoechst 33258, which shares very similar structural motifs with the BIMZ fragment, indicate deviations from coplanarity between the phenol and directly bound benzimidazole to be small at the most (*48*−*50*).

In a geometry-optimized structure using Gausian 03 at the B3LYP/6-31+G** level, the *N*-methylpiperazine ring was also shown to be oriented within the molecular plane of the benzimidazole unit. However, during a CPMD trajectory, the initial in-plane geometry of the *N*-methylpiperazine ring persisted only up to 2.5 ps of the simulation undergoing a ring flip out of the benzimidazole plane. Also, the original conformation was not restored when using this CPMD output geometry in another geometry optimization at the B3LYP/6-31+G** level, and its associated energy confirmed a stable geometry of the CPMD output structure when compared to the in-plane structure. It has to be noted, however, that the energy difference between in-plane and out-of-plane structures was found to be only 1.6 kcal/mol and thus even smaller than the rotational barrier of ethane amounting to 3.0 kcal/mol. Although these calculations were conducted in vacuo and thus cannot be directly transferred to our experimental conditions or the rMD calculations, these results give another indication of a highly flexible *N*-methylpiperazine

substituent at least in the absence of more specific interactions with the DNA.

The role of *N*-methylpiperazine in promoting minor groove binding has been well-documented (*51*), yet discrepancies have arisen regarding the necessity of G·C base pairs for accommodating the bulky *N*-methylpiperazine ring. In two crystal structures of Hoechst 33258, this ring is located in the wider groove near an adjacent G·C base pair, allowing the ring to rotate away from the plane of the benzimidazole (*48*, *50*). However, subsequent solution NMR studies have shown that the bulky *N*-methylpiperazine ring of Hoechst is readily accommodated within the narrow minor groove of an AATT sequence, questioning base pair specific binding of the *N*-methylpiperazine moiety to a GC recognition element (*52*). On the basis of the experimental and theoretical studies presented here, the *N*-methylpiperazine substituent exhibits high flexibility with no clearly defined interactions to the nucleic acid. Being positively charged through protonation under physiological conditions, it is expected to contribute to binding through nonspecific electrostatic interactions with the negatively charged phosphodiester backbone. In addition, a C·G base pair specificity of the *N*-methylpiperazine ring within the PBD hybrid is not indicated by our recent UV melting experiments employing different target duplexes (*11*). Thus, replacing a C·G base pair with a T·A base pair at a corresponding position in a closely related decamer duplex even resulted in a stronger drug binding associated with greater drug-mediated duplex stabilization.

CONCLUSIONS

The NMR structural data confirm strong binding of the PBD hybrid to the minor groove of the DNA duplex, with formation of a covalent bond between the PBD moiety and an exocyclic guanine amino group. The three-dimensional structure also offers details on drug−DNA interactions within the complex, revealing a bound drug that tightly fits into the DNA minor groove. We have recently been engaged in the determination of thermodynamic data for these drugs binding to oligonucleotide duplexes (*11*). The determination of the enthalpic and entropic contribution to binding in these former studies gives important hints for the design of high-affinity DNA binding analogues. On the other hand, the structural data reported here offer a detailed view of specific drug−DNA interactions that contribute to the binding energy but are particularly expected to be critical determinants of sequence selectivity. The PBD−benzimidazole hybrid has been developed with the perspective to enhance antitumor activities of simple alkylating PBD derivatives. Structural modifications of the hybrid aimed at enhancing binding affinity and binding specificity will significantly benefit from a detailed knowledge of the thermodynamics as well as of the three-dimensional complex structure for pinpointing any specific drug−DNA interactions. Therefore, the information gathered can assist in the rational design of improved derivatives of this type of alkylating DNA binding drug in particular and also of DNA recognition by minor groove binding ligands in general.

SUPPORTING INFORMATION AVAILABLE

Proton assignments for the free $d(AACAATTGTT)_2$ duplex and the free PBD−benzimidazole hybrid as well as for the 1:1 drug−DNA complex; experimental H11a(ω_1)−H11(ω_2), H11(ω_1)−H11a(ω_2), and H1(ω_1)−H11a(ω_2) DQF-COSY cross-peaks of the drug−DNA adduct; distribution of NOE-derived intranucleotide and internucleotide distances within the DNA duplex; time-dependent rmsd for snapshots of a restrained molecular dynamics simulation of the drug−DNA complex at 300 K; 2D rmsd plot of the piperazine and benzimidazole atoms for the snapshots taken at 20 ps intervals of the two combined rMD simulations; and glycosidic torsion angle κ and pseudorotation phase angle *P* of nucleotides in the complex. This material is available free of charge via the Internet at http://pubs.acs.org.

REFERENCES

1. Hurley, L. H., and Petrusek, R. L. (1979) Proposed structure of the anthramycin-DNA adduct. *Nature 282*, 529–531.
2. Petrusek, R. L., Anderson, G. L., Garner, T. F., Fannin, Q. L., Kaplan, D. J., Zimmer, S. G., and Hurley, L. H. (1981) Pyrrolo-[1,4]benzodiazepine antibiotics. Proposed structures and characteristics of the in vitro deoxyribonucleic acid adducts of anthramycin, tomaymycin, sibiromycin, and neothramycins A and B. *Biochemistry 20*, 1111–1119.
3. Graves, D. E., Pattaroni, C., Krishnan, B. S., Ostrander, J. M., Hurley, L. H., and Krugh, T. R. (1984) The reaction of anthramycin with DNA. Proton and carbon nuclear magnetic resonance studies on the structure of the anthramycin-DNA adduct. *J. Biol. Chem. 259*, 8202–8209.
4. Bose, D. S., Thompson, A. S., Ching, J., Hartley, J. A., Berardini, M. D., Jenkins, T. C., Neidle, S., Hurley, L. H., and Thurston, D. E. (1992) Rational design of a highly efficient irreversible DNA interstrand cross-linking agent based on the pyrrolobenzodiazepine ring system. *J. Am. Chem. Soc. 114*, 4939–4941.
5. Gregson, S. J., Howard, P. W., Thurston, D. E., Jenkins, T. C., and Kelland, L. R. (1999) Synthesis of a novel C2/C2′-exo unsaturated pyrrolobenzodiazepine cross-linking agent with remarkable DNA binding affinity and cytotoxicity. *Chem. Commun. 9*, 797–798.
6. Kamal, A., Rao, M. V., Laxman, N., Ramesh, G., and Reddy, G. S. K. (2002) Recent developments in the design, synthesis and structure-activity relationship studies of pyrrolo[2,1-*c*][1,4]benzodiazepines as DNA-interactive antitumour antibiotics. *Curr. Med. Chem.: Anti-Cancer Agents 2*, 215–254.
7. Kamal, A., Ramu, R., Tekumalla, V., Khanna, G. B. R., Barkume, M. S., Juvekar, A. S., and Zingde, S. M. (2008) Remarkable DNA binding affinity and potential anticancer activity of pyrrolo[2,1-*c*]-[1,4]pyrrolobenzodiazepine−naphthalimide conjugates linked through piperazine side-armed alkane spacers. *Bioorg. Med. Chem. 16*, 7218–7224.
8. Kamal, A., Ramulu, P., Srinivas, O., Ramesh, G., and Kumar, P. P. (2004) Synthesis of C8-linked pyrrolo[2,1-*c*][1,4]benzodiazepine−benzimidazole conjugates with remarkable DNA-binding affinity. *Bioorg. Med. Chem. Lett. 14*, 4791–4794.
9. Harshman, K. D., and Dervan, P. B. (1985) Molecular recognition of B-DNA by Hoechst 33258. *Nucleic Acids Res. 13*, 4825–4835.
10. Embrey, K. J., Searle, M. S., and Craik, D. J. (1993) Interaction of Hoechst 33258 with the minor groove of the A + T-rich DNA duplex $d(GGTAATTACC)_2$ studied in solution by NMR spectroscopy. *Eur. J. Biochem. 211*, 437–447.
11. Rettig, M., Kamal, A., Ramu, R., Mikolajczak, J., and Weisz, K. (2009) Spectroscopic and calorimetric studies on the DNA recognition of pyrrolo[2,1-c][1,4]benzodiazepine hybrids. *Bioorg. Med. Chem. 17*, 919–928.
12. Hertzberg, R. P., Hecht, S. M., Reynolds, V. L., Molineux, I. J., and Hurley, L. H. (1986) DNA-sequence specificity of the pyrrolo-[1,4]benzodiazepine antitumor antibiotics: Methidium-propyl-EDTA-iron(II) footprinting analysis of DNA-binding sites for anthramycin and related drugs. *Biochemistry 25*, 1249–1258.
13. Krugh, T. R., Graves, D. E., and Stone, M. P. (1989) Two-dimensional NMR studies on the anthramycin-$d(ATGCAT)_2$ adduct. *Biochemistry 28*, 9988–9994.
14. Kopka, M. L., Goodsell, D. S., Baikalov, I., Grzeskowiak, K., Cascio, D., and Dickerson, R. E. (1994) Crystal structure of a covalent DNA drug adduct: Anthramycin bound to C-C-A-A-C-G-T-T-G-G and a molecular explanation of specificity. *Biochemistry 33*, 13593–13610.
15. Antonow, D., Barata, T., Jenkins, T. C., Parkinson, G. N., Howard, P. W., Thurston, D. E., and Zloh, M. (2008) Solution structure of a 2:1 C2-(2-naphthyl) pyrrolo[2,1-*c*][1,4]benzodiazepine DNA adduct: Molecular basis for unexpectedly high DNA helix stabilization. *Biochemistry 47*, 11818–11829.
16. Gottlieb, H. E., Kotlyar, V., and Nudelman, A. (1997) NMR chemical shifts of common laboratory solvents as trace impurities. *J. Org. Chem. 62*, 7512–7515.

17. Goddard, T. D., and Kneller, D. G. (2005) SPARKY 3, University of California, San Francisco.
18. Saenger, W. (1984) Principles of Nucleic Acid Structure, Springer, New York.
19. Case, D. A., Darden, T. A., Cheatham, T. E., III, Simmerling, C. L., Wang, J., Duke, R. E., Luo, R., Merz, K. M., Pearlman, D. A., Crowley, M., Walker, R. C., Zhang, W., Wang, B., Hayik, S., Roitberg, A., Seabra, G., Wong, K. F., Paesani, F., Wu, X., Brozell, S., Tsui, V., Gohlke, H., Yang, L., Tan, C., Mongan, J., Hornak, V., Cui, G., Beroza, P., Mathews, D. H., Schafmeister, C., Ross, W. S., and Kollman, P. A. (2006) AMBER 9, University of California, San Francisco.
20. Pérez, A., Marchán, I., Svozil, D., Sponer, J., Cheatham, T. E.III, Laughton, C. A., and Orozco, M. (2007) Refinement of the AMBER force field for nucleic acids: Improving the description of α/γ conformers. *Biophys. J. 92*, 3817–3829.
21. Wang, J., Wolf, R. M., Caldwell, J. W., Kollman, P. A., and Case, D. A. (2004) Development and testing of a general amber force field. *J. Comput. Chem. 25*, 1157–1174.
22. Bayly, C. I., Cieplak, P., Cornell, W. D., and Kollman, P. A. (1993) A well-behaved electrostatic potential based method using charge restraints for deriving atomic charges: the RESP model. *J. Phys. Chem. 97*, 10269–10280.
23. Cieplak, P., Cornell, W. D., Bayly, C., and Kollman, P. A. (1995) Application of the multimolecule and multiconformational RESP methodology to biopolymers: Charge derivation for DNA, RNA, and proteins. *J. Comput. Chem. 16*, 1357–1377.
24. Hawkins, G. D., Cramer, C. J., and Truhlar, D. G. (1996) Parametrized models of aqueous free energies of solvation based on pairwise descreening of solute atomic charges from a dielectric medium. *J. Phys. Chem. 100*, 19824–19839.
25. Bashford, D., and Case, D. A. (2000) Generalized Born models of macromolecular solvation effects. *Annu. Rev. Phys. Chem. 51*, 129–152.
26. Jorgensen, W. L., Chandrasekhar, J., Madura, J. D., Impey, R. W., and Klein, M. L. (1983) Comparison of simple potential functions for simulating liquid water. *J. Chem. Phys. 79*, 926–935.
27. Darden, T., York, D., and Pedersen, L. (1993) Particle mesh Ewald: An N*log(N) method for Ewald sums in large systems. *J. Chem. Phys. 98*, 10089–10092.
28. Essmann, U., Perera, L., Berkowitz, M. L., Darden, T., Lee, H., and Pedersen, L. G. (1995) A smooth particle mesh Ewald method. *J. Chem. Phys. 103*, 8577–8593.
29. van Gunsteren, W. F., and Berendsen, H. J. C. (1977) Algorithms for macromolecular dynamics and constraint dynamics. *Mol. Phys. 34*, 1311–1327.
30. Shao, J., Tanner, S. W., Thompson, N., and Cheatham, T. E.III (2007) Clustering molecular dynamics trajectories: 1. Characterizing the performance of different clustering algorithms. *J. Chem. Theory Comput. 3*, 2312–2334.
31. Humphrey, W., Dalke, A., and Schulten, K. (1996) VMD: Visual Molecular Dynamics. *J. Mol. Graphics 14*, 33–38.
32. Lavery, R., and Sklenar, H. (1988) The definition of generalized helicoidal parameters and of axis curvature for irregular nucleic acids. *J. Biomol. Struct. Dyn. 6*, 63–91.
33. Lavery, R., and Sklenar, H. (1988) Defining the structure of irregular nucleic acids: Conventions and principles. *J. Biomol. Struct. Dyn. 6*, 655–667.
34. Langel, W., and Menken, L. (2002) Simulation of the interface between titanium oxide and amino acids in solution by first principles MD. *Surf. Sci. 538*, 1–9.
35. Becke, A. D. (1992) Density-functional thermochemistry. I. The effect of the exchange-only gradient correction. *J. Chem. Phys. 96*, 2155–2160.
36. Feigon, J., Wright, J. M., Leupin, W., Denny, W. A., and Kearns, D. R. (1982) Use of two-dimensional NMR in the study of a double-stranded DNA decamer. *J. Am. Chem. Soc. 104*, 5540–5541.
37. Scheek, R. M., Russo, N., Boelens, R., Kaptein, R., and van Boom, J. H. (1983) Sequential resonance assignments in DNA proton NMR spectra by two-dimensional NOE spectroscopy. *J. Am. Chem. Soc. 105*, 2914–2916.
38. Rajagopal, P., Gilbert, D. E., van der Marel, G. A., van Boom, J. H., and Feigon, J. (1988) Observation of exchangeable proton resonances of DNA in two-dimensional NOE spectra using a presaturation pulse: Application to d(CGCGAATTCGCG) and d(CGCGAm6ATTCGCG). *J. Magn. Reson. 78*, 526–537.
39. Wüthrich, K. (1986) NMR of Proteins and Nucleic Acids, John Wiley & Sons, New York.
40. Mountzouris, J. A., Wang, J.-J., Thurston, D., and Hurley, L. H. (1994) Comparison of a DSB-120 DNA interstrand cross-linked adduct with the corresponding bis-tomaymycin adduct: An example of a successful template-directed approach to drug design based upon the monoalkylating compound tomaymycin. *J. Med. Chem. 37*, 3132–3140.
41. Boyd, F. L., Cheatham, S. F., Remers, W., Hill, G. C., and Hurley, L. H. (1990) Characterization of the structure of the anthramycin-$d(ATGCAT)_2$ adduct by NMR and molecular modeling studies. Determination of the stereochemistry of the covalent linkage site, orientation in the minor groove of DNA, and effect on local structure. *J. Am. Chem. Soc. 112*, 3279–3289.
42. Arnott, S., and Hukins, D. W. (1973) Refinement of the structure of B-DNA and implications for the analysis of X-ray diffraction data from fibers of biopolymers. *J. Mol. Biol. 81*, 93–105.
43. Barkley, M. D., Cheatham, S., Thurston, D. E., and Hurley, L. H. (1986) Pyrrolo[1,4]benzodiazepine antitumor antibiotics: Evidence for two forms of tomaymycin bound to DNA. *Biochemistry 25*, 3021–3031.
44. Jenkins, T. C., Hurley, L. H., Neidle, S., and Thurston, D. E. (1994) Structure of a covalent DNA minor groove adduct with a pyrrolobenzodiazepine dimer: Evidence for sequence-specific interstrand cross-linking. *J. Med. Chem. 37*, 4529–4537.
45. Chaires, J. B. (1998) Energetics of drug-DNA interactions. *Biopolymers 44*, 201–215.
46. Haq, I. (2002) Thermodynamics of drug-DNA interactions. *Arch. Biochem. Biophys. 403*, 1–15.
47. Haq, I., Ladbury, J. E., Chowdhry, B. Z., Jenkins, T. C., and Chaires, J. B. (1997) Specific binding of Hoechst 33258 to the d(CGCAAATTTGCG)$_2$ duplex: Calorimetric and spectroscopic studies. *J. Mol. Biol. 271*, 244–257.
48. Pjura, P. E., Grzeskowiak, K., and Dickerson, R. E. (1987) Binding of Hoechst 33258 to the minor groove of B-DNA. *J. Mol. Biol. 197*, 257–271.
49. Teng, M. K., Usman, N., Frederick, C. A., and Wang, A. H. (1988) The molecular structure of the complex of Hoechst 33258 and the DNA dodecamer d(CGCGAATTCGCG). *Nucleic Acids Res. 16*, 2671–2690.
50. Carrondo, M. A., Coll, M., Aymami, J., Wang, A. H., van der Marcel, G. A., van Boom, J. H., and Rich, A. (1989) Binding of a Hoechst dye to d(CGCGATATCGCG) and its influence on the conformation of the DNA fragment. *Biochemistry 28*, 7849–7859.
51. Bostock-Smith, C. E., and Searle, M. S. (1999) DNA minor groove recognition by bis-benzimidazole analogues of Hoechst 33258: Insights into structure-DNA affinity relationships assessed by fluorescence titration measurements. *Nucleic Acids Res. 27*, 1619–1624.
52. Embrey, K. J., Searle, M. S., and Craik, D. J. (1993) Interaction of Hoechst 33258 with the minor groove of the A + T-rich DNA duplex $d(GGTAATTACC)_2$ studied in solution by NMR spectroscopy. *Eur. J. Biochem. 211*, 437–447.